



PHYSICA [

Physica E 40 (2007) 241-244

www.elsevier.com/locate/physe

Electron transport in thin graphite films: Influence of microfabrication processes

Takuya Moriki^a, Akinobu Kanda^{a,d,*}, Takashi Sato^a, Hisao Miyazaki^{b,d}, Shunsuke Odaka^{b,c}, Youiti Ootuka^a, Yoshinobu Aoyagi^{c,d}, Kazuhito Tsukagoshi^{b,d}

^aInstitute of Physics and TIMS, University of Tsukuba, Tsukuba 305-8571, Japan

^bThe Institute of Physical and Chemical Research (RIKEN), Wako 351-0198, Japan

^cInterdisciplinary Graduate School of Science and Engineering, Tokyo Institute of Technology, Yokohama 226-8502, Japan

^dJapan Science and Technology Agency, CREST, Kawaguchi 332-0012, Japan

Available online 14 June 2007

Abstract

We experimentally investigated electron transport in thin graphite films including tens of graphene layers. The samples were fabricated by mechanical peeling of graphite, e-beam lithography, metal deposition and lift-off. For some samples, Ar-ion bombardment was carried out prior to the metal deposition to enhance the electrical transparency of the contacts. We found that the Ar-ion bombardment significantly deteriorate the samples; the electron transport changes from the semimetallic behavior to the weak-localization behavior. © 2007 Elsevier B.V. All rights reserved.

PACS: 73.63.-b; 81.05.Uw; 73.23.-b; 73.20.Fz

Keywords: Graphene; Graphite; Universal conductance fluctuation; Weak localization

1. Introduction

Thin graphite films including a single layer (graphene) has attracted much attention not only due to their unique electronic properties but also due to their potential application to nanoelectronic devices. It is just a few years ago that successful formation of thin films by mechanical peeling and microfabrication of electrodes allow one to observe electric field effect [1,2] and unconventional quantum Hall effect [3,4]. For the further study of this system, the microfabrication processes should be optimized, but to our knowledge, systematic study has not been done yet. Here, we focus on this point and investigate experimentally the effect of microfabrication processes on the electron transport of thin graphite films.

2. Experimental

We used a grain of natural graphite (size ~ 1 mm) as the starting material. Following the standard procedure [1], we mechanically exfoliated the grain with adhesive tape and placed the produced thin films on a substrate. As a substrate, we used highly doped Si wafer with a 300-nm layer of SiO₂ on the top. By judging from colors of the graphite films under the optical microscope, we chose thin graphite films with thickness of about 10 nm, which looked violet against the background of reddish violet. A 10 nm graphite film corresponds to ~ 30 layers of graphene.

Here, we prepared three types of samples (I–III). For type-I samples, metal electrodes (Pd(5 nm)/Al(100 nm) or Ti(5 nm)/Al(100 nm)) were placed on thin graphite films by using standard e-beam lithography, metal deposition, and lift-off. Fig. 1(a) is a scanning electron microscope (SEM) image of a type-I sample. In the fabrication of type-II samples, Ar-ion bombardment (1 keV, Ar pressure of $9 \times 10^{-4} \, \mathrm{Pa}$, 1 min) was carried out prior to the metal

^{*}Corresponding author. Fax: +81298535081. *E-mail address:* kanda@lt.px.tsukuba.ac.jp (A. Kanda).

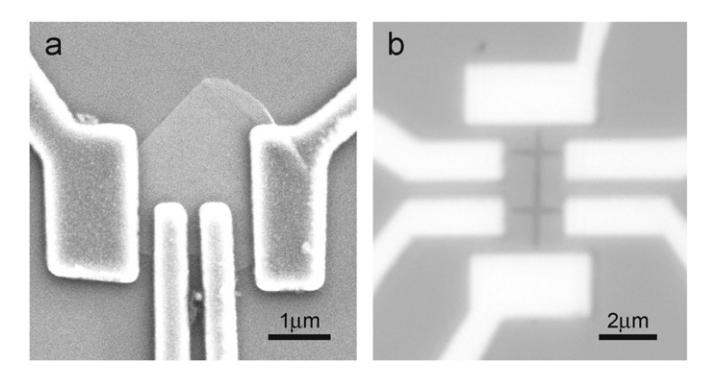


Fig. 1. (a) A SEM image of a type I sample. (b) A optical microscope image of a type-III (Hall bar) sample. The linewidth is about 0.3 µm.

deposition, but the other processes were the same as those for the type-I samples. The Ar-ion bombardment is a widely used technique to enhance the electrical transparency of metal contacts. Note that part of the graphite film which does not contact the metal electrodes was covered with the e-beam resist (PMMA) during the bombardment. For the type-III samples, the films were partially etched with oxygen plasma with PMMA as a mask to form a Hall bar (see Fig. 1(b)) or a ring after the processes for the type-II samples.

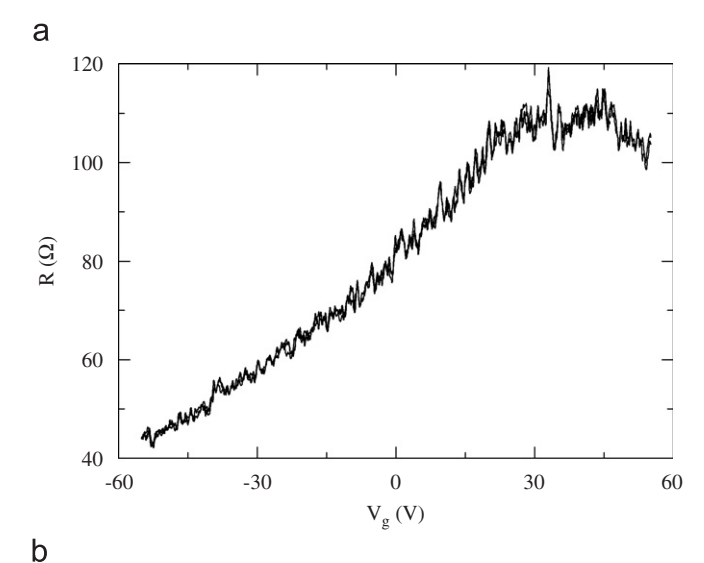
Electron transport properties were measured by the four terminal method in a dilution fridge. We examined two type-I samples, three type-II samples and four type-III samples. Zero-bias resistance (ZR) was measured using a lock-in method with an excitation frequency of 17 Hz, while differential conductance was obtained by numerically differentiating I-V characteristics. Gate-voltage ($V_{\rm g}$) was applied through a highly doped Si substrate as a back gate. Magnetic field was applied perpendicular to the graphite films.

In the measurement, no indication of the superconducting proximity effect was observed below the superconducting transition temperature of the Al electrodes (~1.3 K), presumably because of poor transparency of the graphite–electrode interfaces, large separation between electrodes, and/or disorder in the graphite films.

3. Results

3.1. General features

Fig. 2 shows the $V_{\rm g}$ -dependence of ZR (electric field effect) and the magnetoresistance for a type-I sample at 40 mK. The overall $V_{\rm g}$ - and B-dependencies are almost the same for all samples (type I–III): The ZR had a peak structure as a function of the gate voltage, superimposed by reproducible fluctuations (universal conductance fluctuations (UCF)). The peak is due to the band structure of graphite with slightly overlapping conduction and valence band (semimetal). The magnetoresistance was positive for all gate voltages, again superimposed by the UCF structures. The positive magnetoresistance is characteristic to systems with coexisting hole and electron carriers [5]. In



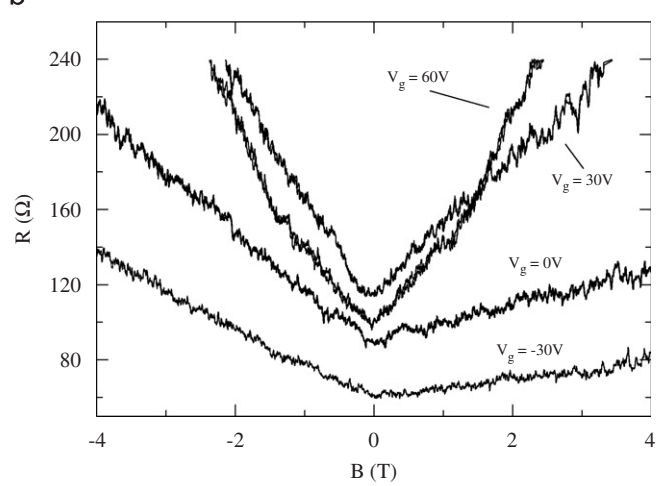


Fig. 2. Electric field effect (a) and magnetoresistance (b) for a type-I sample at 40 mK. The overall characteristics were common to all samples. In (a), data for three $V_{\rm g}$ sweeps are shown, which are almost identical. All structures, including small resistance fluctuations, are reproducible.

some samples, the magnetoresistance was asymmetric with respect to B=0, as shown in Fig. 2(b). The origin of this asymmetry is not clear at this moment.

3.2. Type-I samples

Fig. 3(a) shows the temperature dependence of ZR for the same sample as in Fig. 2. Above 10 K ZR decreases with increasing temperature, while below 10 K it looks almost independent of temperature, on the resistance scale in the figure. But when we look at the temperature dependence in more detail (Fig. 3(b)), we notice that the amplitude of UCF increases with decreasing temperature even below 10 K, eliminating the possibility that the Joule heating is responsible for the weak temperature dependence of ZR below 10 K.

The constant ZR at low temperatures can be interpreted as a signature of semimetal. Assuming that the conductance is proportional to the carrier density and

Download English Version:

https://daneshyari.com/en/article/1547746

Download Persian Version:

https://daneshyari.com/article/1547746

Daneshyari.com